(2)

NAVAL POSTGRADUATE SCHOOL
Monterey, California

THESIS

A POWDER X-RAY DIFFRACTION STUDY
OF
TWO ALUMINUM-LITHIUM BASED ALLOYS

by

Te-Kang Wang

March 1991

Thesis Advisor: Alan G.Fox

Unclassified

Security Classification of this page

REPORT DOCUMENTATION PAGE

1a Report Security Classification: Unclassified	1b Restrictive Markings
2a Security Classification Authority	3 Distribution Availability of Report: Approved for public release; distribution is unlimited.
2b Declassification/Downgrading Schedule	
4 Performing Organization Report Number(s)	5 Monitoring Organization Report Number(s)
6a Name of Performing Organization: Naval Postgraduate School; 6b Office Symbol: 34	7a Name of Monitoring Organization: Naval Postgraduate School
6c Address (city, state, and ZIP code): Monterey, CA 93943-5000	7b Address (city, state, and ZIP code): Monterey, CA 93943-5000
8a Name of Funding/Sponsoring Organization; 8b Office Symbol (If Applicable)	9 Procurement Instrument Identification Number
8c Address (city, state, and ZIP code)	10 Source of Funding Numbers: Program Element Number; Project No; Task No; Work Unit Accession No

11 Title (Include Security Classification)
A POWDER X-RAY DIFFRACTION STUDY OF TWO ALUMINUM-LITHIUM BASED ALLOYS

12 Personal Author(s) Te-Kang Wang

13a Type of Report	13b Time Covered	14 Date of Report (year, month,day)	15 Page Count
Master's Thesis	From To	1991 March	63

16 Supplementary Notation The views expressed in this thesis are those of the author and do not reflect the official policy or position of the Department of Defense or the U.S. Government.

17 Cosati Codes			18 Subject Terms (continue on reverse if necessary and identify by block number)
Field	Group	Subgroup	Aluminum-Lithium Alloys, Microstructural development, X-ray Diffraction.

19 Abstract (continue on reverse if necessary and identify by block number

The microstructures of solution treated, quenched and aged Al-2.5 wt.%Li and Al-2.0 wt.%Li-2.76 wt.%Mg-1.03 wt.%Cu alloys were studied by powder X-ray diffraction. The as-quenched alloys showed extensive X-ray line broadening due to particle size effects and the intensity measurements indicated a significant amount ordering in the as-quenched state. These results were interpreted using a `spinodal ordering' model which suggests that Al-Li-based alloys order during quenching and then spinodally decompose into regions of order and disorder so that the final microstructure comprises small ordered regions(size ~ 40 nm) in a disordered matrix.Studies on the aged Al-2.5 wt.%Li alloy indicated that after initial short-time aging, the δ' particle growth follows Ostwald ripening kinetics in agreement with previous work. Studies on the aged quaternary alloy indicated that T_1 and S phases grow at the expense of δ' in this system so that δ' precipitates are not a dominant strengthening mechanism in this alloy.

20 Distribution/Availability of Abstract	21 Abstract Security Classification
[X] unclassified/unlimited [ ] same as report [ ] DTIC users	Unclassified
22a Name of Responsible Individual: Alan G. Fox	22b Telephone (Include Area code): (408) 646-2142 / 22c Office Symbol: ME / FX

DD FORM 1473, 84 MAR 83 APR edition may be used until exhausted

All other editions are obsolete

security classification of this page

Unclassified

Approved for public release; distribution is unlimited.

A Powder X-Ray Diffraction Study

of

Two Aluminum-Lithium Based Alloys

by

Te-Kang Wang
Captain, Republic of China Army
B.S., Chung Cheng Institute of Technology, 1984

Submitted in partial fulfillment of the requirements
for the degree of

MASTER OF SCIENCE IN MECHANICAL ENGINEERING

from the

NAVAL POSTGRADUATE SCHOOL
March 1991

Author: Te-Kang Wang
Te-Kang Wang

Approved by: A. G. Fox
Alan G. Fox, Thesis Advisor

Anthony J. Healey, Chairman
Department of Mechanical Engineering

ABSTRACT

The microstructure of solution-treated, quenched and aged Al-2.5 wt.%Li and Al-2.0 wt.%Li-2.76 wt.%Mg-1.03 wt.%Cu alloys were studied by powder X-ray diffraction. The as-quenched alloys showed extensive X-ray line broadening due to particle size effects, and the intensity measurements indicated a significant amount of ordering in the as-quenched state. These results were interpreted using a 'spinodal ordering' model, which suggests that Al-Li-based alloys order during quenching and then spinodally decompose into regions of order and disorder so that the final microstructure comprises small ordered regions (size ~ 40 nm) in a disordered matrix. Studies on the aged Al-2.5 wt.%Li alloy indicated that after initial short-time aging, the δ' particle growth follows Ostwald ripening kinetics in agreement with previous work. Studies on the aged quaternary alloy indicated that T_1 and S phases grow at the expense of δ' in this system so that δ' precipitates are not a dominant strengthening mechanism in this alloy.

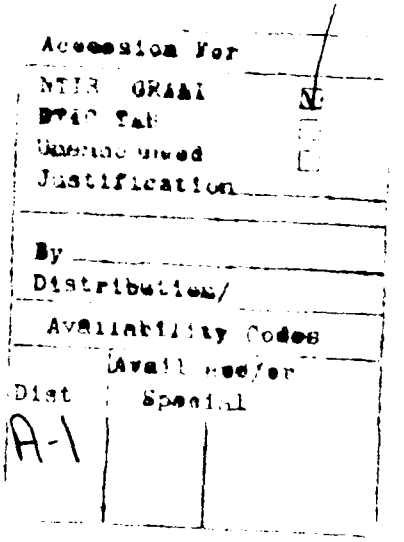

TABLE OF CONTENTS

LIST OF TABLES

LIST OF FIGURES

ACKNOWLEDGEMENTS

I would like to express my gratitude to Professor Alan G. Fox for patiently providing insight and direction in this research endeavor. I am also grateful to Professor Terry McNelley for providing the samples for this study. I wish to thank Miss Eiizabeth R. Grayson EIT for her technical support, and Lts. Larry Comerford and Steve Cade for their help in proofreading. A special thank-you goes to my wife, Anny Chiu, for her patience, understanding, and encouragement during my studies at the Naval Postgraduate School.

I. INTRODUCTION

In the past few years, aluminum-lithium alloys have been studied extensively for aerospace and military applications because they provide a combination of high strength, increased elastic modulus, low density, resistance to stress corrosion cracking, thermal stability, improved performance, and cost efficiency. Al-Li-based alloys are considered to be superior to graphite-epoxy composite materials for aircraft skin applications since the composite possesses drawbacks such as fiber anisotropy, low fracture toughness, difficulty in inspection, susceptibility to environmental degradation, and high cost of manufacture. These composite materials are used extensively in airframes due to their weight-saving characteristics, however.

Lithium additions to aluminum greatly increase stiffness and yield strength. However, these superior properties in Al-Li alloys are always accompanied by decreasing ductility, low fracture resistance, and poor toughness in peak-aged and overaged conditions. The major strengthening mechanism of Al-Li alloys is the precipitation and aging of a hardening phase. This metastable phase is called $\delta'(Al_3Li)$; the formation mechanism and coarsening behavior of this phase are not completely understood.

The mechanical properties are strongly dependent on alloy composition and microstructural properties, including particle size distribution of matrix and precipitates, interactions between microstructure and dislocations, volume fraction of precipitates, and the deformation mode. The optimum microstructure to improve toughness can be achieved by appropriate lithium additions, adding alloy elements, or thermomechanical processing methods. Thus, many systems more complex than Al-Li (binary), such as Al-Li-X (ternary) and Al-Li-Mg-X (quaternary), have been developed and in

Although many researchers have tried to examine the microstructure of Al-Li-based alloys via transmission electron microscopy (TEM), the present work will be conducted mainly by the X-ray diffraction method (XRD). Whitman and Fuller at NPS have used XRD to analyze Al-2.5 wt.%Li-.15 wt.%Zr (plate samples) and Al-4.1 wt.%Li (plate and powder samples) alloys respectively and determined the particle size at the as-quenched and early aging stage using the Scherrer equations [Ref. 1, 2]. Texture effects were observed by comparing the plate samples with powder samples. This work will aim to characterize the δ' phase by performing XRD studies on two kinds of Al-Li-based alloys (Al-2.5 wt.%Li-.15 wt.%Zr, Navalite: Al-2.0 wt.%Li-2.76 wt.%Mg-1.03 wt.%Cu-.12 wt.%Zr) using powder samples filed from the as-quenched and aged alloys.

II. BACKGROUND

A. ALUMINUM-LITHIUM-BASED ALLOYS

1. Development History

The pursuit of competitive age-hardenable alloys with higher strength, better formability, and improved resistance to fatigue and corrosion has been ongoing since the development of the heat treatable aluminum alloy Duralumin prior to World War I. The development of Al-Li-based alloys has been underway for more than 65 years. It is noticeable that Li is one of just eight elements with considerable solubility in aluminum as a solid solution (exceeding 1 at.%, e.g. 4.2 wt.% in Al-Li binary alloy) [Ref. 3].

The first aluminum alloy containing lithium for structural applications, Sclern, was introduced in Germany in the early 1920s. However, the consequent developments in Al-Li-based alloys were surpassed by the improved Duralumin type alloys. A high-strength alloy was discovered by I. M. LeBaron in 1942 and a patent granted for an Al-Cu-Li-X alloys in 1945. Once again, the merits of Al-Li-based alloys were ignored for about ten years due to the discovery of high-strength alloy 7075 (Al-Zn-Mg-Cu) in 1943 [Ref. 3].

In 1958, the Alcoa 2020 alloy provided a high strength-to-weight ratio, increased elastic modulus, and resistance to exfoliation corrosion and stress corrosion cracking. It was successfully used for skins on the wing and horizontal stabilizer of the U.S. Navy RA-5C Vigilante aircraft. Unfortunately, major problems with the 2020 alloy were its low ductility and unacceptable fracture toughness, which was lower than tnat of 7075-T6 alloys. As a result of these limitations of 2020, use of this alloy was reduced in the late 1960s. [Ref. 3]

At the same time, the Soviet Union made efforts to develop Al-Li-based alloys (e.g., AL-Mg-Li) with lithium additions in excess of 2 wt.%, resulting in alloy 01420. This alloy was later applied on the MIG-25 Foxbat [Ref. 4]. The USSR workers also studied Al-

Zn-Mg-Li alloy systems for weldable applications. The actual mechanism of strengthening first identified in Al-Li and Al-Cu-Li alloys by Silcock was not of great importance before the 1970s.

Since the introduction of TEM techniques, development and research have emphasized the transformation of precipitate phases and deformation behavior related to microstructure. Research into developmental Al-Li alloys was rapidly promoted by the aircraft industry's ever-increasing need for faster speed, high performance, greater payload, current production skills, and competition with advanced composite materials.

2. Current Status

Commercial aluminum-lithium alloys and two conventional (non-lithium-containing) aluminum alloys have been developed in recent years. Their compositions are shown in Table 1.

TABLE 1. ALUMINUM-LITHIUM AND CONVENTIONAL ALLOY COMPOSITIONS (Nominal Weight %) [Ref. 4]

alloy	Li	Cu	Mg	Mn	Zr	Zn	Cr
2090	2.2	2.8	--	--	0.1	--	--
8091	2.6	2.0	0.9	--	0.1	--	--
2091	2.0	2.2	1.5	--	0.1	--	--
8090	2.5	1.3	1.0	--	0.1	--	--
2024	--	4.4	1.5	0.6	--	--	--
7075	--	1.6	2.5	--	--	5.6	0.2

The alloying elements Cu, Mg, and Zr are added to modify the Al-Li microstructure and to provide additional strengthening (solution or dispersion hardening). These elements modify microstructure either by altering Li solubility in Al, by forming Cu-rich and Mg-rich phases, or by co-precipitating with $\delta'(Al_3Li)$. The replacement of conventional alloys guides the work on Al-Li alloy design; usually lightness and rigidity are the major properties concerned. In addition, in Al-Li alloys, design has to satisfy several

technological requirements:

* casting ability into larger size ingots
* hot and cold work ability
* recycling compatibility
* no abrupt change in production skills and maintenance and repair

Al-Li alloys were developed by Pechiney to satisfy the strength offered by conventional Al alloys with a density reduction of 8 to 12 percent. The Al-Li-Cu-Mg-Zr system has become the most promising [Ref. 5]. The major current commercial application for Al-Li alloy 2090 is extensive usage on Boeing airplanes as well as other Boeing products. Another example of wide use of Al-Li is the French Airbus body family A310, A320 and A300-600 [Ref. 5, 6].

Testing for military applications has also been conducted:

* The U.S. Air Force F15D wing skin, using the 8090 alloy, produced a weight saving of 24 pounds while increasing the panel's performance.
* F15-E 9g spectra have been increased with 8090 to extend fatigue life. This was tested for the first time in 1986 [Ref. 7].

The U.S. Naval Air Development Center is also combining its efforts with Alcoa Inc. to achieve the special goal of replacing 7075 alloys with 8089 or 2090 series alloys. For maximum strength, 7075-T6 will be compared with 2090-T8E41; for high stress corrosion resistance, 7075-T73 will be compared with 8092 or 2090.

3. Benefits and Drawbacks of Al-Li Alloys

The introduction of new advanced materials with higher strength, light weight, and thermal stability contributes to the development of new aerospace transportation vehicles for higher performance, greater payload, and better fuel economy. Among these materials, Al-Li alloys are obviously the most attractive candidates for aerospace applications for several reasons. These are:

* *Formability.* Current machinery and skills are well developed. It is not necessary to spend extra money on establishing new techniques.

* *Resource availability.* Reserves indicate that the lithium supply is substantial for the present market and for several decades of development [Ref. 3].

* *Design.* The inspection methods and test procedures are well established. Knowledge of Al alloys in engineering design has been systematically recognized. Several decades of experience and well-balanced response in the overall engineering of aluminum alloys provide an outstanding advantage [Ref. 8].

* *Reliability and Safety.* Aluminum alloys have shown their superiority to composite materials in plane crash performance. The composite materials have a higher tendency to splinter [Ref. 6].

* *Superplasticity.* Elongations in Al-Li alloys exceeding one thousand percent can be achieved by means of thermal mechanical processing. Thus more complicated shapes can be produced without difficulty with Al-Li alloys [Ref. 9].

* *Weldability.* An ultra-high-strength, forgeable Al-Cu-Li-Ag-Mg alloy has been found with good weldability and a strong natural aging response without prior cold work to stimulate precipitation of the second phase [Ref. 10].

The major shortcoming of Al-Li alloys is low toughness, particularly in the aged condition, and much research work is being directed at this. The list of disadvantages includes:

* *The low toughness problem.* Coarsening phases promote precipitate free zones near grain boundaries, resulting in intergranular fracture failure on overaged material, particularly in the short transverse direction.

* *Investment.* Aluminum-lithium alloys need special techniques to prevent loss of Li, as it is very reactive and corrosive during production. The cost of production may be 2-4 times higher than that of conventional alloys, but it is still

competitive with regard to other advanced materials such as composites [Ref. 11].

* *Scrap segregation.* Al-Li scrap must be kept separated from conventional aluminum alloys. This can be considered a minor problem [Ref. 5].

B. MICROSTRUCTURE

1. Phase Diagram

For binary Al-Li alloys, the phase diagram was proposed as in Figure 1 [Ref. 12]. δ' is a metastable phase with an $L1_2$ cubic structure. Another intermediate phase is the body-centered cubic Al-Li δ phase.

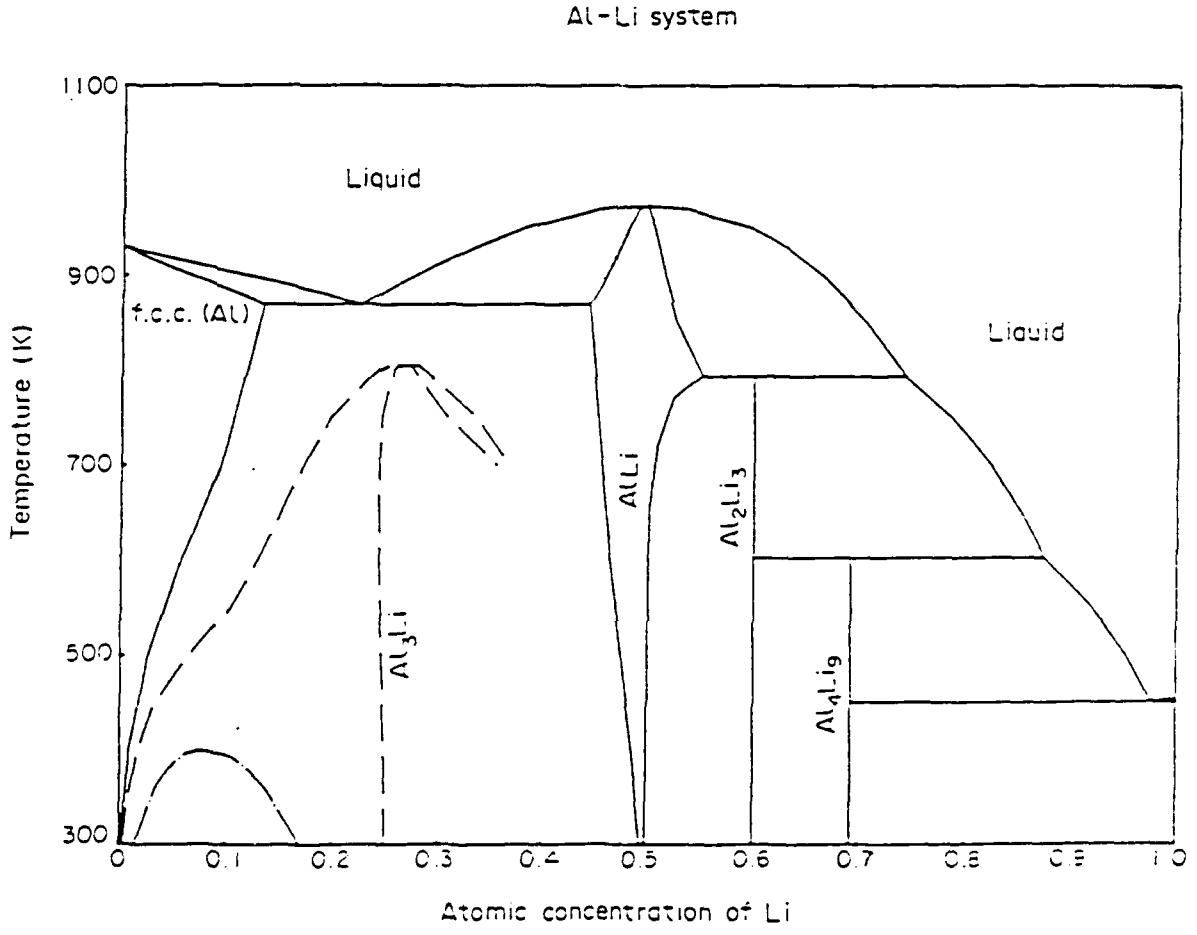

Figure 1. Al-Li Phase Diagram [Ref. 12].

2. Phase Description

a. $\delta'(Al_3Li)$

When a homogeneous α solid solution is quenched into the metastable two-phase region as shown in Figure 2, the δ' precipitate forms in the disordered α matrix, referred to as a superlattice structure. δ' is a metastable phase with an ordered $L1_2$ structure and a lattice parameter of 4.045Å, as shown in Figure 3. The spherical precipitates in the aged alloys are coherent and have a cube/cube orientation, with the matrix showing almost no misfit (less than 0.1%). The stoichiometric composition of δ' is considered to be Al_3Li [Ref. 13].

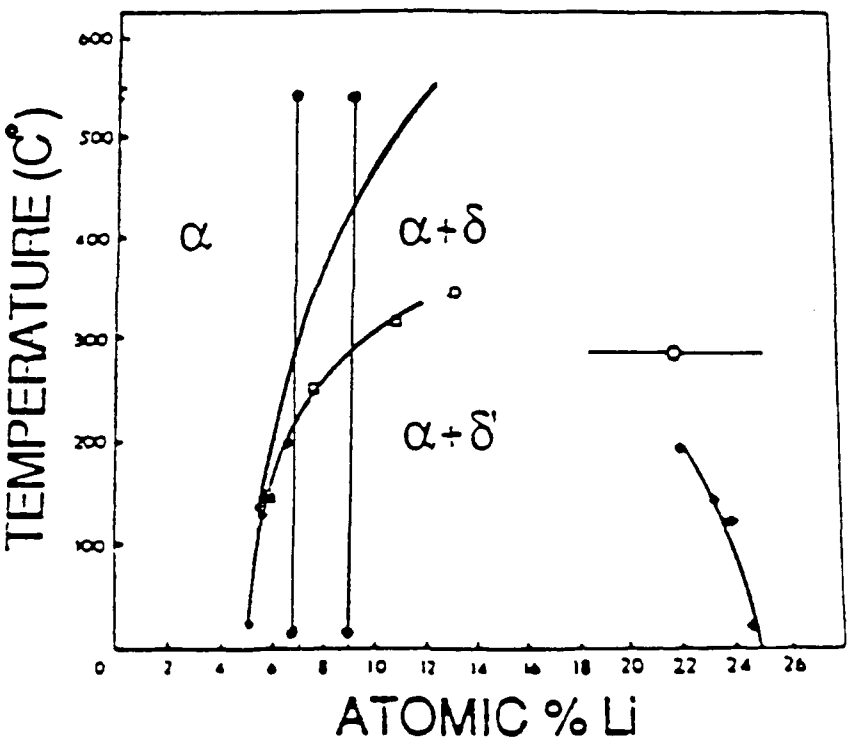

Figure 2. Miscibility Gap region of Al-Li Phase Diagram: Vertical bars demonstrate quench for Navalite (left) and Binary (right).

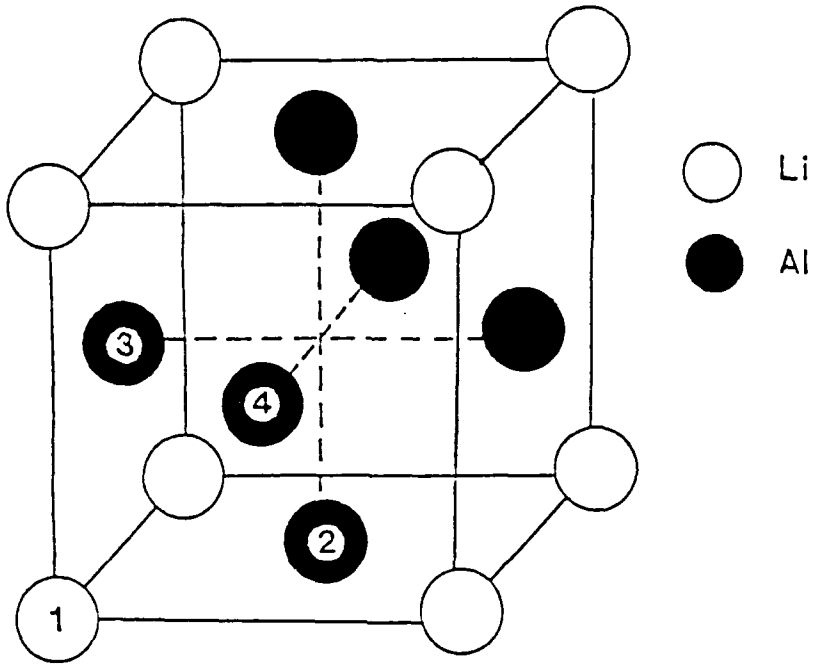

Figure 3. L1₂ Ordered Structure of $\delta'(Al_3Li)$.

The increase in strength on aging is attributed to the interaction between δ' precipitates and superlattice dislocations in the parent phase [Ref. 14]. Coherent δ'-particles are sheared by moving dislocations, resulting in an intense planar slip responsible for low ductility during plastic deformation [Ref. 15]. The morphology of δ' is dependent on Li content and aging time. For longer aging times or lower Li-content alloys, particles are more likely to be spherical. The growth of δ' obeys Ostwald ripening kinetics in that the average radius of particle increases proportionally to $(\text{time})^{1/3}$ while the total particle number reduces to maintain a constant volume fraction.

Increasing the Li content accelerates the particle coarsening rate. The larger particles grow at the expense of the smaller ones to reduce the free energy related to the decreasing surface area of particles as growth proceeds. The particle size distribution (PSD) can be modeled by the Weibull distribution equation. The PSD in the binary alloys varies with

the lithium content. Small volume fractions (0.12) show negatively skewed PSDs. However, increasing the δ' volume fraction to 0.55 leads to a positively skewed PSD [Ref. 16]. The Lifshitz-Slyozov Encounter Modified (LESM) theory was the only one accurate in modeling the PSD of δ', although the other theories also predict a broadening of PSD with increasing volume fraction of precipitates. The LESM model assumes coalescence occurring between any two particles that are close to each other and indicates that anti-phase boundaries (APBs) would appear in δ' particles when there is a high volume fraction of precipitates. [Ref. 17]

b. δ(AlLi)

The coarse equilibrium δ phase has a lattice parameter of 6.37Å. It is an intermetallic compound with a cubic B32 (NaTl) type structure. The formation mechanism of δ is not well understood. It is believed that δ forms preferentially along high-angle grain boundaries during the early stages of aging and is nucleated within the parent phase after longer aging times [Ref. 18]. It has been reported that δ can be removed from the sample during electropolishing, making it difficult to observe in the electron microscope [Ref. 19].

Niskanel et al. proposed that δ nucleates from the preferential coarsening of δ' [Ref. 20]:

$$\alpha \rightarrow \delta' \rightarrow \delta$$

Although no positive evidence for δ formation in as-quenched Al-Li alloys exists in the literature, Whitman has observed the presence of δ in the as-quenched state for the Al-2.5 wt.%Li-0.15 wt.%Zr alloy [Ref. 1]. Williams also suggested that δ forms independently of δ' and nucleates heterogeneously within the matrix and along grain boundaries [Ref. 21]:

$$\alpha \rightarrow \delta$$

The dissolution of the δ' precipitates occurs near grain boundaries and contributes to the growth of δ on aging. It is related to the growth of δ' precipitate free zones (PFZs) that has been observed adjacent to grain boundaries [Ref. 18]. The coarsening PFZ leads to poor toughness after longer-time aging.

c. Co-precipitates

In the Al-Li-Mg system, strengthening is provided by co-precipitates in addition to the δ' phase. The ternary Al_2MgLi precipitate forms along grain boundaries during artificial aging. Its sequence is as follows:

$$\alpha \rightarrow \delta'(Al_3Li) \rightarrow Al_2MgLi \text{ (equilibrium phase).}$$

The addition of magnesium reduces the solubility of lithium during early aging and promotes coherent δ' precipitation [Ref. 22]. In the Al-Li-Cu system, copper additions result in increasing ductility and the T_1 phase contributes to increasing yield and tensile strength of the alloy. Its formation sequence is:

$$\alpha \rightarrow \delta'(Al_3Li) \rightarrow T_1(Al_2CuLi)$$

For the Al-Li-Mg-Cu system, the precipitation of $T_1(Al_2CuLi)$ and $S(Al_2CuMg)$ phases occurs. The S phase has been shown to encourage homogenous deformation by dispersing slip [Ref. 23]. Magnesium and copper improve the overall strength of a binary alloy by modifying the microstructure with co-precipitates forming in the matrix and/or grain boundaries in ternary or more complex systems.

Zr additions are made to retard recrystallization, suppress grain growth, reduce planar slip on deformation due to shearable precipitates, and promote δ' precipitation. Al_3Zr has an f.c.c., $L1_2$ structure and a small misfit with the α matrix. The Al_3Zr particles do not dissolve in the Al-Li solid solution at normal solution treatment temperatures. As a result, they can act as nucleation sites for δ' precipitation [Ref. 24].

3. Current Precipitation Theory

Various methods such as thermal analysis, TEM, and small angle X-ray scattering (SAXS) have verified the existence of δ'. TEM work by many researchers has revealed superlattice reflections in as-quenched alloys. δ' precipitation is inevitable when the alloy lithium content exceeds 5.5 at.%, if solution heat treatment is followed by a quench to a low temperature state [Ref. 25]. The ordered phase can also be detected by X-ray diffraction techniques with analysis of the superlattice reflections. [Ref. 26]

Williams and Edington investigated δ' formation in 1975. There are two ways that δ' can be considered to form: by conventional nucleation and growth, or by spinodal decomposition. If spinodal decomposition is occurring, the predicted ordered phase should show X-ray sideband structures and satellites on the diffraction patterns. As no diffraction satellites were seen, however, the weak intensity of the sideband compared to the fundamental (only 1/600) indicates that spinodal decomposition is a possible mechanism for the formation of δ' [Ref. 27]. The most interesting region of the phase diagram is where the metastable and stable phases coexist, as in Figures 4 and 5, and has been investigated by different workers.

Gayle and Vandersande suggested that the $\alpha \rightarrow \delta'$ transformation is first-order and a two-phase field is thus thermodynamically required. They suggested the phase diagram in Figure 4 [Ref. 28]. The Cluster Variation Method has been used by Sigli and Sanchez to study the stable and metastable phase equilibria in Al-Li alloys via a free energy model. They concluded a metastable miscibility gap is predicted as shown in Figure 5, by assuming that δ' is formed from G.P. zones. However, δ' already exists in the as-quenched state so that evolution of δ' from G.P. zones does not seem to be correct. [Ref. 29]

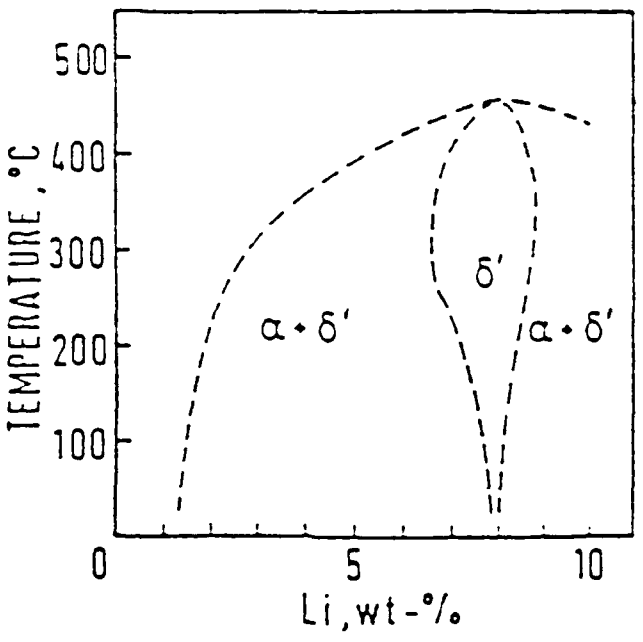

Figure 4. Metastable $\alpha+\delta'$ phase region proposed by Gayle and Vandersande [Ref. 28].

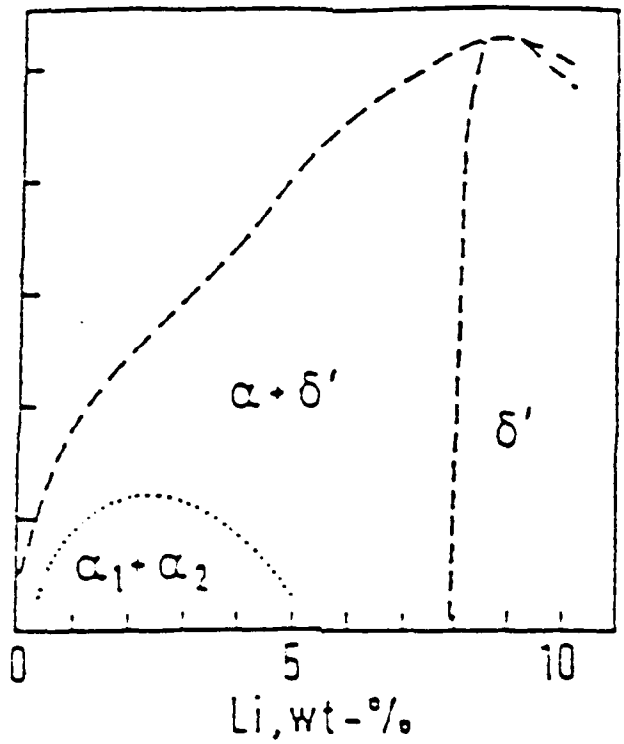

Figure 5. The Miscibility Gap predicted by Sigli and Sanchez [Ref. 29].

Figure 6 shows a different theoretical model, proposed by Khachaturyan in 1986. The quench process is A → D → E. From an unstable region, that is, a disordered solution of composition A, congruent ordering to B is unstable with respect to spinodal decomposition. Consequently, from B → C there is spinodal decomposition and also from C → D (disordered phase), due to the Li-lean ordered phase. Another way is B → E, a spinodal decomposition process to a Li-rich ordered phase [Ref. 25]. High-resolution election microscopy (HREM) can easily reveal the ordered phase regions that are surrounded by disordered matrices, as Radmilovic, Fox, and Thomas have shown [Ref. 26, 30]. These results suggest that the spinodal decomposition after congruent ordering is the transformation path during quenching of Al-Li alloys, as described above. Spooner also studied the radius of δ' precipitates during the early stages of aging and suggested that the formation of δ' is associated with spinodal decomposition. [Ref. 31]

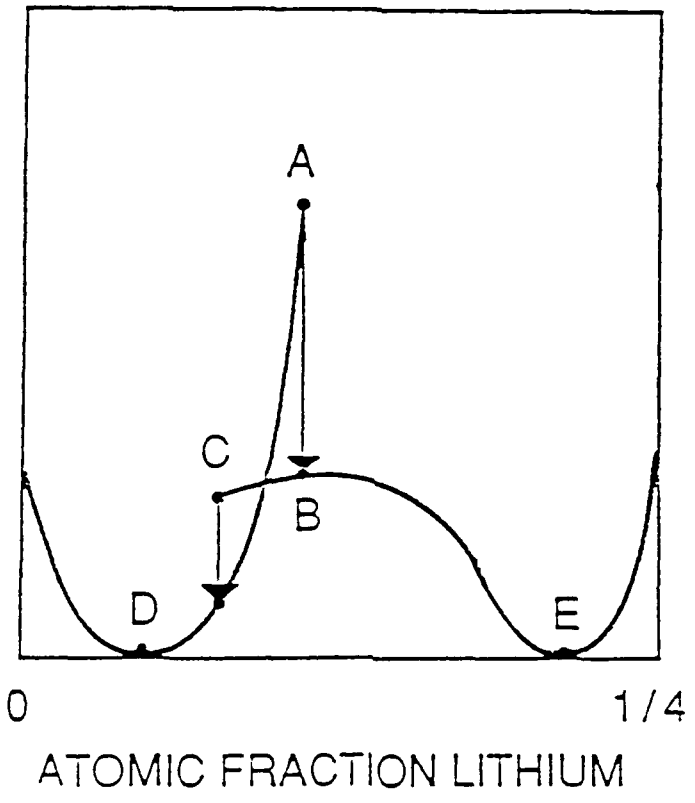

Figure 6. Spinodal Decomposition Model proposed by Khachuturyan et al. [Ref. 25].

4. Strengthening Mechanisms

The intrinsic strengthening mechanism of Al-Li alloys is due to the presence of lithium in solid solution and also to the presence of fully or partially coherent ordered precipitates in the matrix. For every 1 wt.% addition of lithium to aluminum up to 4 wt.%, the density is reduced by 3% and the elastic modulus increased by 6%. It is not surprising that Li can offer large density reductions when the atomic mass of Li (6.94) and Al (26.98) are compared. Lithium also provides the extraordinary feature of increasing the elastic modulus, as shown in Figure 7 [Ref. 32]. This can be explained as follows. Fox and Fisher suggested that electronic structure dominates this kind of behavior. They found the nearest-neighbor

(n.n.) distance of an Al-Li solution (2.86Å) is smaller than that of pure lithium (3.031Å). This implies that there is a higher bonding force between nearest-neighbor Al-Li atoms, i.e., a higher Debye temperature and higher elastic modulus due to the addition of lithium to aluminum. Thus, the elastic modulus increases as the Li content increases [Ref. 33, 34].

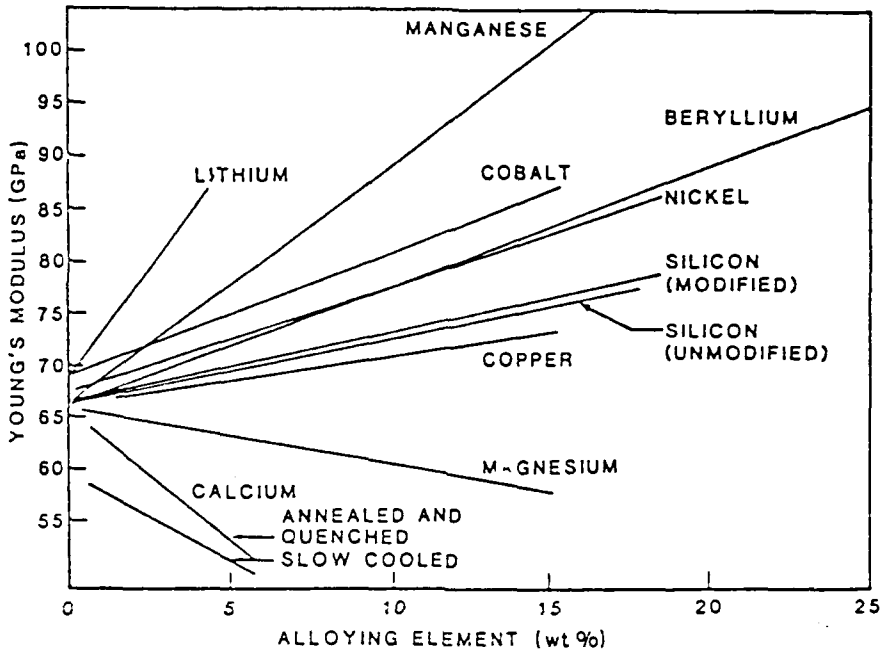

Figure 7. The effects of elements on the elastic modulus of aluminum alloys [Ref. 32].

The interaction of dislocations with precipitates is considered to be the major contributor to strength increases in Al-Li alloys. For underaged to peak strength Al-Li alloys, the shear mechanism dominates the behavior for the critical sizes of particles between 300Å and 500Å [Ref. 15]. For overaged alloys, the δ' particles are too large for dislocations to cut through and Orowan loops form, resulting in decreased strength. Noble et al. have suggested that order hardening (creation of APBs) or the combination of order hardening and elastic modulus strengthening are the main contributors to maximum strength in the peak aged state [Ref. 35].

The increased strength of δ' is considered to be responsible for low toughness and poor ductility. The strength of sheared particles has been increased by dislocations cutting

through the particles and by the stress field which is built up. This leads to dislocation pile-up. The poor fracture toughness and low ductility are a result of strain localization by inhomogeneous planar slip at grain boundaries or in the matrix.

Sanders and Starke found that fracture occurs transgranularly for short-time aging. However, for longer-time aging, failure occurs intergranularly due to PFZ coarsening [Ref. 36]. Furukawa et al. also showed that for greater than 11.0 at.% Li, the planar slip that occurs at low lithium was not found and other mechanisms for low ductility should have been taken into account [Ref. 15].

5. Methods for Analysis

The microstructure of an Al-Li alloy is often difficult to analyze because Li has a low atomic number. Chemical analysis is difficult due to toxicity and reactivity. Although there are various qualitative and quantitative techniques available, the study is still limited by the fact that δ' particles are often too tiny to be detected and Li in δ' is metastable. Therefore, no universal method can apply to the present study. However, any quantitative technique should have a spatial resolution of less than 500Å and the ability to detect less than 3.0 wt.% lithium [Ref. 37:p. 337].

The following is a summary of some of the qualitative and quantitative methods:

* *Atom Probe Field Ion microscopy (APFIM).* APFIM is very powerful in many areas since it can analyze all elements with equal efficiencies. However, since APFIM can only detect very small volumes of samples (~ $10^{-16}m^3$), it is better to combine this with TEM to obtain convincing results [Ref. 38].
* *Convergent Beam Election Diffraction (CBED).* A small composition change will result in a change in lattice parameter of δ' during aging. This was found by Sung et al. using CBED to detect the composition changes in Al-Li alloys. However, this is an indirect method which limits its data interpretation. [Ref. 37:p. 343]

* *Electron Energy Loss Spectroscopy (EELS).* The minimum detectable mass fraction of Li in Al is estimated to be about 10.3 at.% (2.7 wt.%) in EELS, as discussed by Chan and Williams [Ref. 39]. The sensitivity is not sufficient to examine lower Li concentrations. Plasmon EELS demonstrated an ability to detect small changes in Li content on a sub-10nm scale. This requires a high-resolution, high-dispersion spectrometer (e.g., retarding field type), and binary alloy standards are hard to generate.

* *Transmission Electron Microscopy (TEM).* TEM can be used to determine particle size, especially of δ'. The major shortcoming is the limitation of the too-small sample size for statistical sampling, which cannot be used to obtain all of the information about precipitation kinetics, volume fractions, or PSD, as reported by Spooner. TEM combined with small angle X-ray scattering gives satisfactory results. [Ref. 31]

* *X-ray Diffraction (XRD).* XRD can provide information about lithium content. Determination of the particle size and volume fraction of precipitates and detection of the different phases in large volumes of sample can be performed by XRD. This work will focus on XRD analysis.

C. FUNDAMENTAL PRINCIPLES OF X-RAY DIFFRACTION

1. General Basis

Bragg's law provides the basis for X-ray diffraction:

$$n\lambda = 2d\sin\theta \qquad (1)$$

λ: Wavelength of incident radiation.

θ: The angle of reflection.

d: The interplanar spacing.

For a specific plane (hkl), d is defined as (in cubic materials):

$$d = \frac{a_0}{\sqrt{h^2 + k^2 + l^2}} \qquad (2)$$

a_0 : The lattice parameter of cubic crystal.

For any given compound and desired plane, d can be calculated via θ determined from the position of diffracted peaks.

Many factors will affect the XRD results, such as the intensity of diffraction and the broadening of diffraction profiles [Ref. 2]. The intensity of diffracted beams can be expressed as:

$$I^{(hkl)} = Kp\phi^{(hkl)} [F^{(hkl)}]^2 \qquad (3)$$

K: A constant of proportionality.

p: The multiplicity factor.

ϕ: The Lorentz-polarization factor.

$$\phi = \frac{1 + \cos^2\theta}{\sin^2\theta\cos\theta} \qquad (4)$$

F: The structure factor, which usually includes the temperature factor.

2. Particle Size Determination

Particle size can be determined by analyzing the diffraction profiles. There are many complicated methods for analyzing diffraction profiles, such as iterative folding techniques and Fourier Transform methods. However, the Scherrer equation will be used in the present analysis to measure the profile width. The Scherrer equation can be written as:

$$L = \frac{K\lambda}{\beta\cos\theta} \qquad (5)$$

L: Particle diameter in Å.

K: A constant = 1.075.

θ: Bragg's reflection angle.

λ: X-ray wavelength in Å.

β: Pure diffraction profile in radians.

In order to calculate the particle size L, the pure diffraction profile β should be expressed as below, assuming the line shape to be Gaussian:

$$B^2 = b^2 + \beta^2 \qquad (6)$$

B: Experimentally measured width from diffraction profile.

b: Instrumental factor obtained from analyzing a suitable standard.

B can be defined as the full width at half maximum, or as the integral breadth (Area to height ratio).

3. Calculation of Volume Fraction

The volume fraction of δ' can be obtained by comparing the intensities of two peaks that are diffracted by the fundamental and the superlattice structure. The X-ray structure factors will be introduced first. For a B-rich B_3A $L1_2$ alloy (e.g. δ'), a sites will occupied by A atoms, and b sites are the locations of B atoms in the fully-ordered stoichiometric alloy. If the alloy is disordered, the atoms and sites could be interchanged. The structure factors for this situation can be expressed as below: (7)

$$F_F^{\alpha(\delta')} = \bar{f}[3\exp(-M_b) + \exp(-M_a)] + 0.75\Delta fS[\exp(-M_b) - \exp(-M_a)]$$

$$F_S^{\delta'} = \bar{f}[\exp(-M_b) - \exp(-M_a)] + 0.25\Delta f S[3\exp(-M_b) + \exp(-M_a)] \quad (8)$$

$F_F^{\alpha(\delta')}$ - *fundamental of* $\alpha(\delta')$ $f_{A(B)}$ - *free atom form factors*

$F_S^{\delta'}$ - *superlattice of* δ' $\bar{f} = m_A f_A + m_B f_B$

$M_{a(b)}$ - *temperature factor* $m_{a(b)}$ - *atomic fraction of* $A(B)$

$\Delta f = f_B - f_A$ S - *long range order parameter*

S *must satisfy* $0 \le S \le S_{max}$

$$S_{max} = \frac{3}{4} m_B \qquad \text{for } m_A \ge 0.25$$
$$S_{max} = 4 m_A \qquad \text{for } m_A \le 0.25$$

For a B-rich alloy, assuming $M_a = M_b = M$, equations (7) and (8) can be reduced to:

$$F_F^{\alpha(\delta')} = 4\,(m_A^{\alpha(\delta')}\, f_A + m_B^{\alpha(\delta')}\, f_B)\exp(-M) \quad (9)$$

$$F_S^{\delta'} = S_{max}(f_B - f_A)\exp(-M) \quad (10)$$

X-ray intensities are proportional to the volume fraction V_f and the overall structure factors:

$$F_S^2 = V_f(F_S^{\delta'})^2 \quad (11)$$

$$F_P^2 = (1 - V_f)(F_F^{\alpha})^2 + V_f(F_P^{\delta'})^2 \quad (12)$$

By taking the ratio of the 100 and 200 intensities shown in equation (3) and substituting equations (11) and (12), the volume fraction can be calculated:

$$\frac{I_{100}}{I_{200}} = \frac{\phi^{100}}{\phi^{200}}\left[\frac{F_{s,100}}{F_{F,200}}\right]^2 \quad (13)$$

$I_{100(200)}$ = *Measured experimental intensity of* 100(200)

$\phi^{100(200)}$ = *Lorentz-polarization correction factors*

D. SCOPE OF PRESENT WORK

The δ' precipitates in as-quenched Al-Li alloys and growth characteristics during aging have been studied with TEM and other techniques by many workers. However, the small sampling size, combined with lithium electropolishing losses, limit TEM's effectiveness. Previous work conducted by Whitman [Ref. 1] and Fuller [Ref. 2] has concluded that the δ' features can be effectively monitored by XRD analysis and that powder samples give better results without the preferred orientation effects of plate samples. This study will conduct XRD using two Al-Li based alloys with powder samples to achieve the following objectives:

* To compare the results of powder samples with the plate samples used by Whitman in order to verify the preferred orientation effect.
* To investigate the as-quenched and early aging characteristics using powder samples filed from plate samples which have been heat-treated in various conditions.
* To determine the particle size and volume fraction from XRD data.
* To compare the results obtained from two different composition samples:
  (1) Al-2.5 wt.%Li binary alloy.
  (2) Navalite: Al-2.0Li-1.03Cu-2.76Mg quaternary alloy (in weight percent).

III. EXPERIMENTAL PROCEDURE

A. SAMPLE PREPARATION

1. Alloy Composition and Heat Treatment

The two Al-Li based alloys samples were:

(1) A hot rolled 0.056 in. thick sheet designated P54. with composition Al-2.5Li-0.15Zr (in weight percent).

(2) Navalite, an as-cast aluminum alloy stock number 606172A (N4) with composition Al-2.0Li-1.03Cu-2.76Mg-0.12Zr (in weight percent). Samples were cut into small sheets.

The heat treatments were undertaken in a nitrogen atmosphere to reduce oxidation attributed to the alloys' reactivity. Samples were solution-treated at 540°C for 25 minutes, after which they were rapidly ice-brine quenched, and then placed in a freezer to prevent natural aging. The aging heat treatment was conducted using plate samples at 190°C under nitrogen gas for various times ranging from 2 minutes to 1 hour. The as-quenched and aged samples' surfaces were ground and carefully polished to remove any natural surface strain and oxidation layer during heat treatment.

2. Powder Samples

Powder samples were filed from the treated samples. Plate samples were carefully filed at liquid nitrogen temperatures for about 3 minutes after the samples were submerged into liquid nitrogen for sufficient time to cool them down, especially for as-quenched samples. This reduced the effect of heating and cold work during filing and kept the sample cold, thus preventing natural aging. The powder samples were collected after the filed samples passed through a U.S. standard #325 sieve (45 microns).

B. X-RAY DIFFRACTION

The XRD experimental equipment included a Phillips XRG3100 X-ray generator with a copper target (wavelength 1.5405Å) and a Norelco data control and processor. A 30kV, 35mA power setting and a scan rate of 4 minutes running for 1 degree was suitable for collecting all data.

Powder samples were mounted into a sample holder. The powder was mixed with acetone, pressed into the sample holder, and again wetted with acetone. A razor blade was used to remove the excess powder on the sample holder. The final step consisted of using a final layer of acetone to settle and clean the residual powder around the holder.

C. TEM

3mm diameter discs were punched out of the sectioned samples that were cut from the as-quenched Navalite with a diamond saw. A solution of 35% butoxy ethanol, 3% perchloric acid, and 62% ethanol was used for electropolishing. The Tenupol method was used with 40V, 30mA and a temperature of -40•C.

A JEOL 100 TEM, with voltage setting 120kV, was used to investigate the sample. Photographs were taken of bright and dark field images and diffraction patterns.

IV. RESULTS AND DISCUSSION

A. DATA ANALYSIS

1. Particle Size Calculations

The Scherrer equation (eq. (5)) was used to determine particle size. First, the pure diffraction profile was calculated from equation (6). The experimentally measured breadth B was then determined by the integral breadth method using the equation:

$$B(radians) = \left[\frac{A}{H}\right]\left[chartspeed\left(\frac{degrees}{inches}\right)\right]\left[\frac{2\pi}{360}\right] \qquad (14)$$

A: Area (in.^{2}) of the profile measured.

H: The height (in.) of the peak measured from profile after removing the background.

The area was calculated by weighing the paper cut from the diffraction profile. The mass of the chart paper was 2.5529×10^{-2} grams per square inch, with a standard deviation of 4.128×10^{-4}. By assuming the physical strain broadening of the peaks to be zero due to the very small misfit strain of the δ' in the α matrix, the value of b was determined using instrumental breadths obtained using a quartz standard. The results are tabulated in Appendix C [Ref. 2].

2. Volume Fraction

The volume fraction of δ' can be obtained from solving equation (13). The intensity was calculated as follows:

$$Intensity(counts) = \left[\frac{A}{chartspeed}\right]\left[\frac{Full\ Scale\ Intensity}{verticalscale(inches)}\right]$$

A: Area of profile measured (in.^{2}).

Chartspeed (in./sec).

Full Scale Intensity (counts per sec.).

The following summation was used to determine the free atoms factors:

$$f = \sum_{i=1}^{4} a_i \exp\left[-b_i\left(\sin^2\frac{\theta}{\lambda^2}\right)\right] + C \qquad (16)$$

The value of a_i, b_i and C were obtained from [Ref. 42]. The f can be calculated from equation (16). The results were:

$$f_{Al}^{100} = 10.6442 \qquad f_{Li}^{100} = 2.0422$$

$$f_{Al}^{200} = 8.5077 \qquad f_{Li}^{200} = 1.6314$$

The alloys contain a small amount of zirconium, which can be ignored in the calculations and in the as-quenched state. It is reasonable to assume that the disordered α and ordered δ' have the same composition. The atom fractions are thus:

$$m_{Al}^{\alpha} = m_{Al}^{\delta'} = 0.909$$

$$m_{Li}^{\alpha} = m_{Li}^{\delta'} = 0.901$$

The Lorentz-polarization correction can be determined using eq. (4).

B. AS-QUENCHED RESULTS

Appendices A and B contain tables showing intensity, integral breadth, volume fraction, and particle size results of all conditions for Al-Li binary and Navalite. The summary of as-quenched results of these Al-Li based alloys is found in Table 2.

TABLE 2. SUMMARY OF AS-QUENCHED RESULTS (BASED ON I_{100} / I_{200})

	Al-Li binary	Navalite
ordered phase particle size diameter(Å)	43.3	38.58
Volume fraction	0.51	?
I_{100}	4700	5279
I_{200}	194721	156716
I_{110}	3923	--
I_{220}	144401	120123

TEM micrographs were taken from as-quenched Navalite as shown in Figures 8 and 9. Small precipitates were revealed, but it was very difficult to measure the particle size because of the large number of them contributing to the image.

Figure 8. Bright Field TEM micrograph of as-quenched Navalite with g= (200). The δ' precipitates are very small and difficult to see. Note the dislocation was found in matrix.(100K ×)

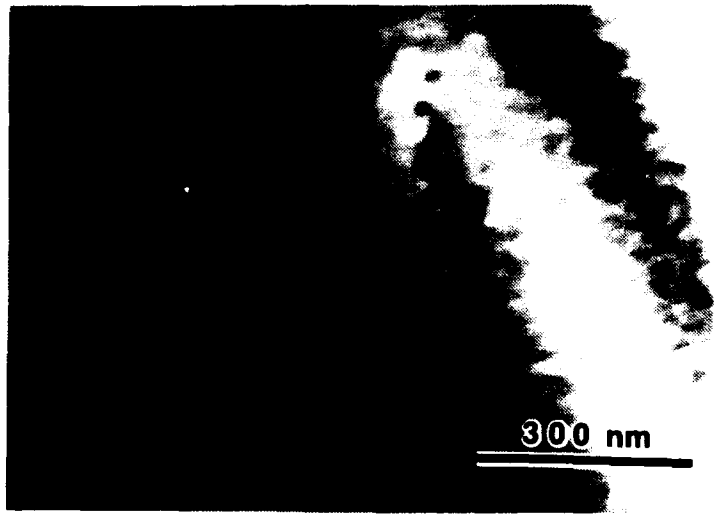

Figure 9. 100 Dark Field TEM micrograph of as-quenched Navalite. The δ' particles are hard to distinguish.

The 100 δ' peak was present in both alloys, but it was very broadened due to particle size effects. It was, however, possible to measure this broadening and the associated particle size. The 100 δ' peak for Navalite was broader than Al-Li binary and so the particle size of the ordered phase in Navalite was therefore smaller than in binary.

In the binary alloy, the 110 superlattice overlapped extensively with the 111 fundamental peak. As a result, an underestimation of intensity measurement on both peaks led to a higher particle size prediction using the Scherrer equation. The comparison of δ' particle radius based on I_{100} and I_{110} is shown in Figure 8 on the previous page. Therefore, the 100 results should be considered closer to the real particle size. The δ' particle size found using the powder sample is 43Å, which is greater than the particle size of the plate sample found by Whitman to be 28Å [Ref. 1]. The difference in size was due to the effects of preferred orientation of the plate samples and experimental error.

The volume fraction of δ' in the binary alloy was found to be 50.5% with a long-range order parameter of 0.36. This is larger than that of plate sample (25.3%). This suggests that the plate sample possibly loses lithium at the surface during heat treatment. Also, there is no texture effect intrinsic in the powder sample. Thus 50.5% of the as-quenched alloy comprises ordered δ' particles with a 43Å particle size. This is surrounded by a disordered matrix with an average particle size of 680Å. This high degree of order, which cannot be quenched out, suggests that congruent ordering followed by spinodal decomposition is the transformation path adopted in quenched alloys as proposed by Khachaturyan et al. [Ref. 25].

The ordered phase in as-quenched Navalite has a 38Å particle size. The volume fraction of the ordered phase could not be calculated precisely due the unknown contribution of the Mg and Cu atoms to F_S^{100} and F_F^{200}.

Assuming a binary composition, the ordered phase volume fraction was 1.03 in Navalite. This is probably because higher Z atoms (such as Mg and Cu) are contributing to the structure factors in an unknown way. [This may be due to the large errors in intensity measurement

and reduction of F_P^{200} due to magnesium atoms.] However, the results (V_f=1.03±0.1), as well as line broadening of the fundamental peaks, suggest that the alloy is nearly fully ordered after quenching. The line-breadth comparison based on the fundamental diffraction profile for these two alloys also indicates that Navalite has a smaller particle size. The Mg and Cu additions have apparently subdued the dissociation of the fully ordered solution into regions of order and disorder. Why this is so is not clear.

C. AGING CHARACTERISTICS

Powder samples directly filed from aged samples give excellent XRD results when compared with either plate samples or aged powder samples from the as-quenched plate samples. Although the preparation of powder samples filed from the aged samples is time-consuming, it prevents lithium losses occurring at the surfaces of the samples.

For the Al-Li binary alloy, the growth of δ' obeys the Ostwald ripening theory. Figures 11 and 12 show good agreement with Ostwald coarsening kinetics. In Figure 11, the line intercept is not equal to zero, suggesting that perhaps the order-disorder transformation or spinodal decomposition dominates the growth kinetics instead of the conventional nucleation and growth mechanism right after quenching. In Figure 10, the 100 δ' radius increases as aging time increases. However, the 110 δ' radius in the early aging (5-10 minutes) showed a small decrease. This may arise because the lithium concentration in the ordered phase has decreased and, perhaps, a spinodal decomposition in fast coarsening matrix is followed by the nucleation of more stable δ' with a smaller size, thus reducing the average particle radius [Ref. 31]. However, the 110 δ' peaks overlapped with 111 fundamentals, perhaps resulting in higher particle size results, particularly for the as-quenched alloy. The I_{100} / I_{200} and I_{110} / I_{220} ratios are plotted against time in Figures 13 and 14. These indicate that the volume fraction of δ' is decreasing as the particles coarsen.

The 111 radius for Navalite and Al-Li binary versus aging time is plotted in Figure 15.

The radius of Navalite was smaller than Al-Li binary; the Navalite particle size coarsening rate was slower than Al-Li also. These results suggest that alloying elements such as magnesium and copper have retarded diffusion rates in Al-Li alloys.

δ 111 peaks were observed in as-quenched and throughout all aging processes for the Al-Li binary alloy. The volume fraction of δ is very small in the as-quenched sample and does not affect the calculations for volume fraction and particle size of δ'. Thus it is possible that the presence of δ did not oppose the nucleation of δ' in the as-quenched state. However, the amount of δ phase increases as the aging time increases.

For Navalite, the δ' peak rapidly disappeared upon aging. The δ' was replaced by other metastable phases such as T_1 (Al_2CuLi) and S(Al_2CuMg). The S phase is considered to be responsible for the reduction of strain localization and PFZ effects.

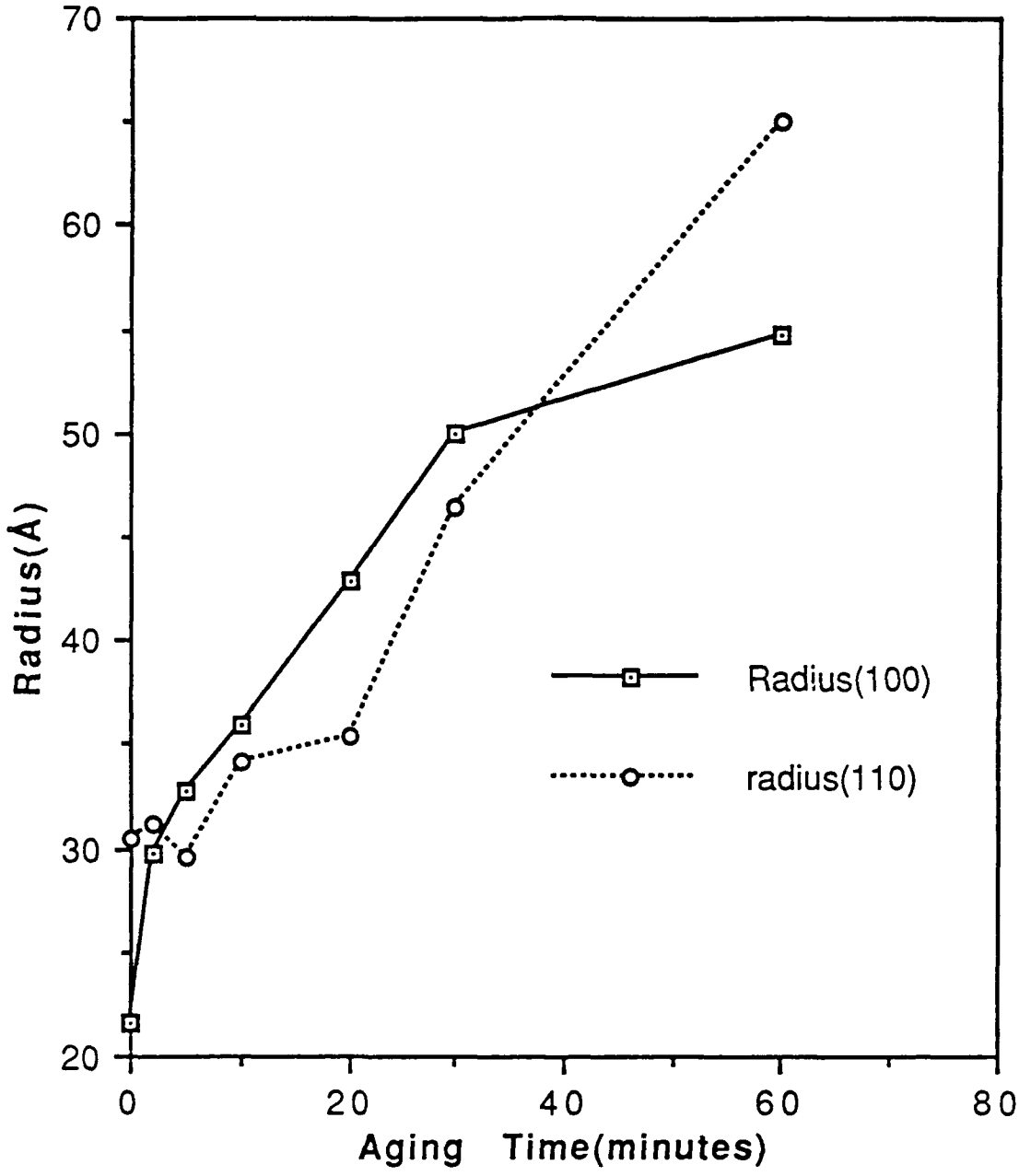

Figure 10. δ' Radius versus Aging Time (Al-Li binary).

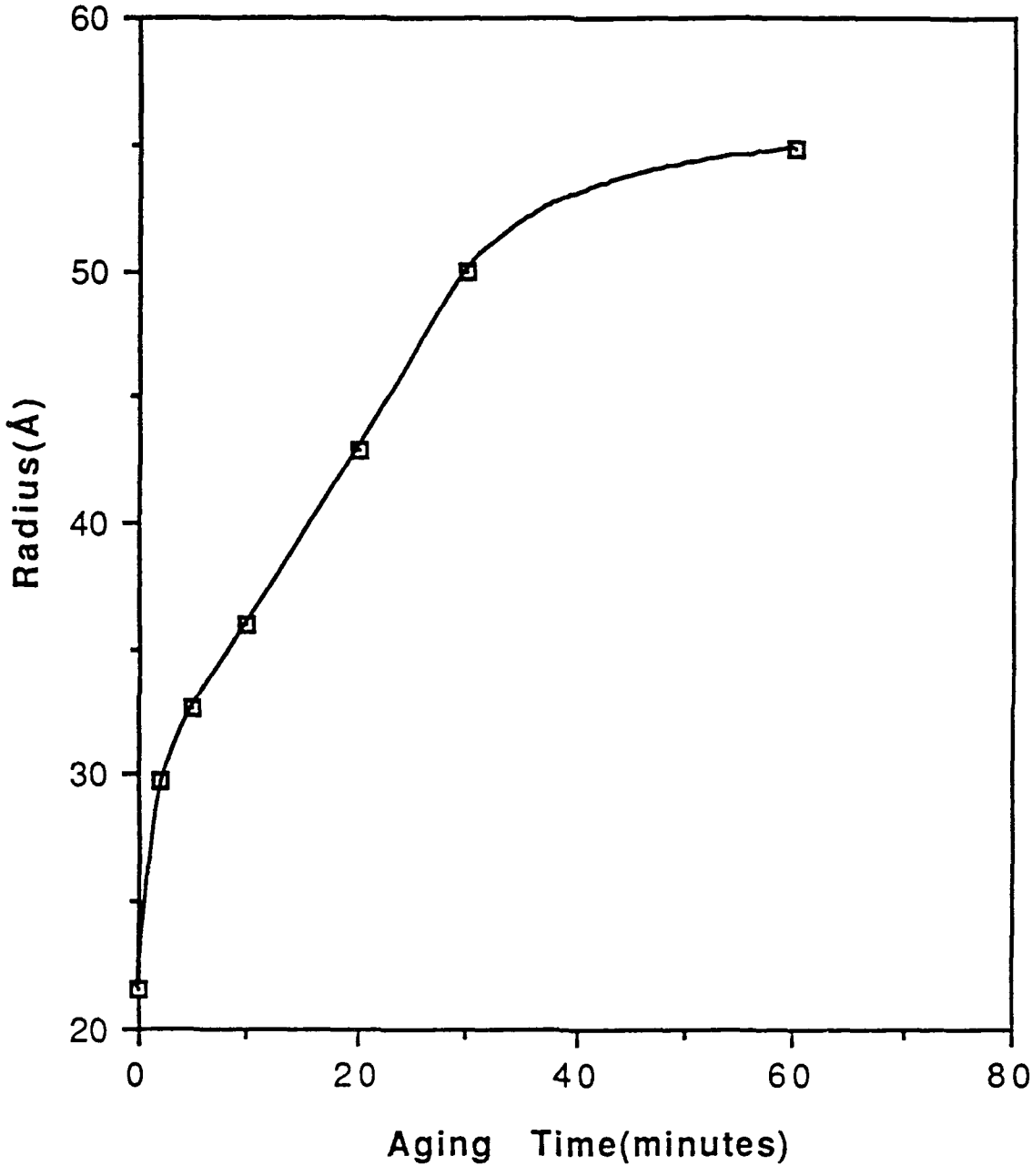

Figure 11. δ' Radius versus Aging Time (Al-Li binary).

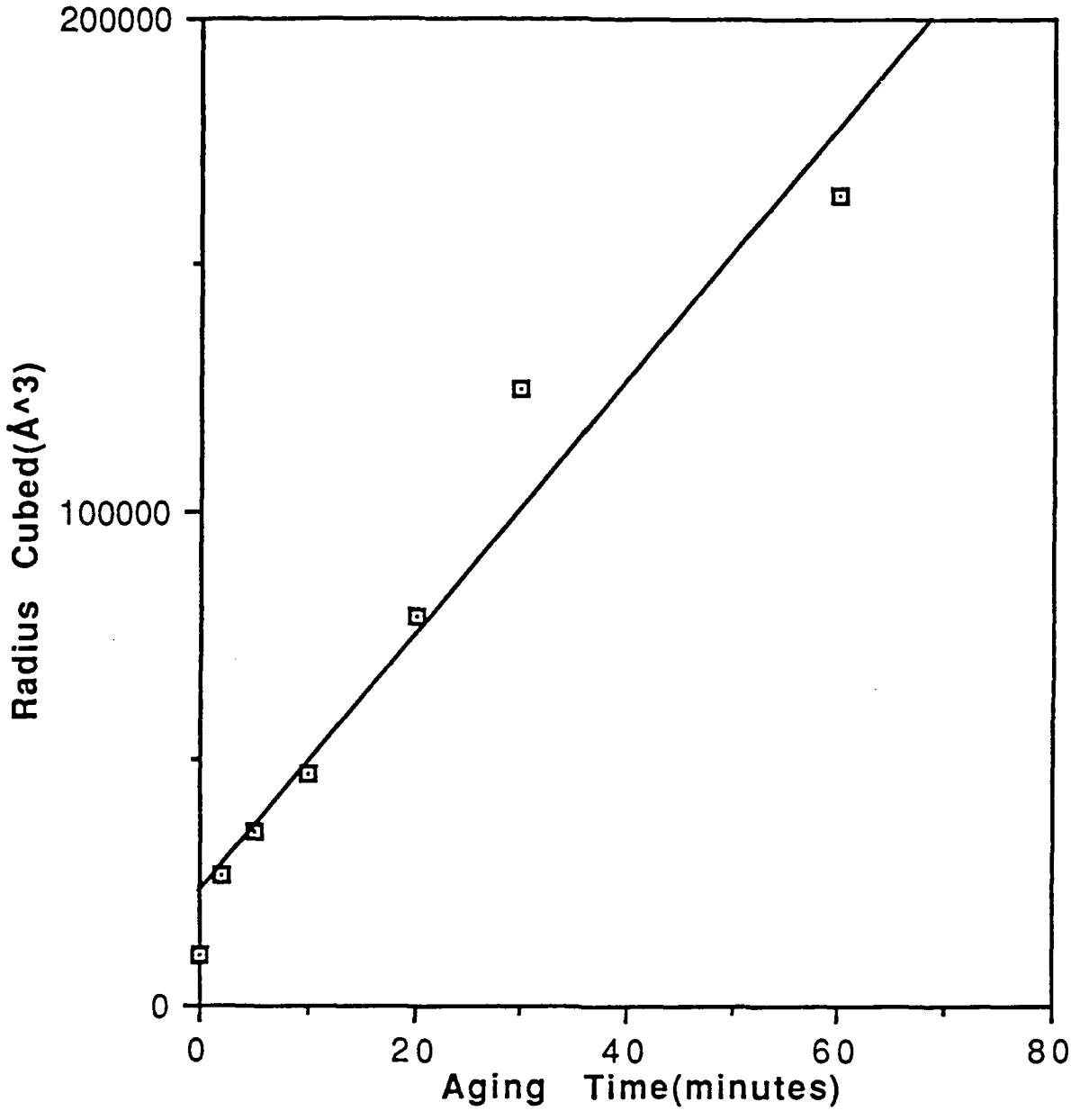

Figure 12. δ' Radius Cubed versus Aging Time (Al-Li binary).

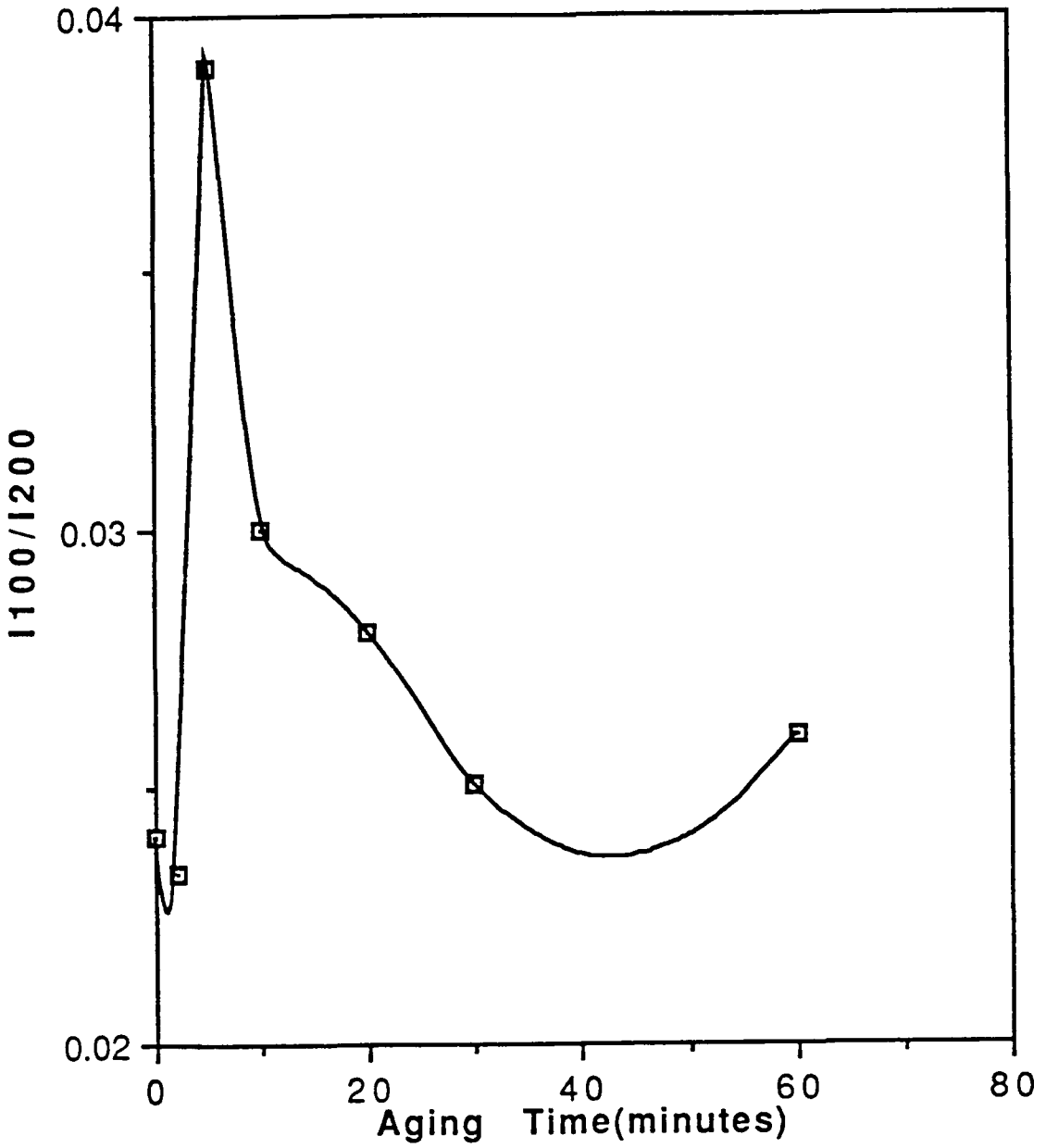

Figure 13. I_{100} / I_{200} versus Aging Time (Al-Li binary).

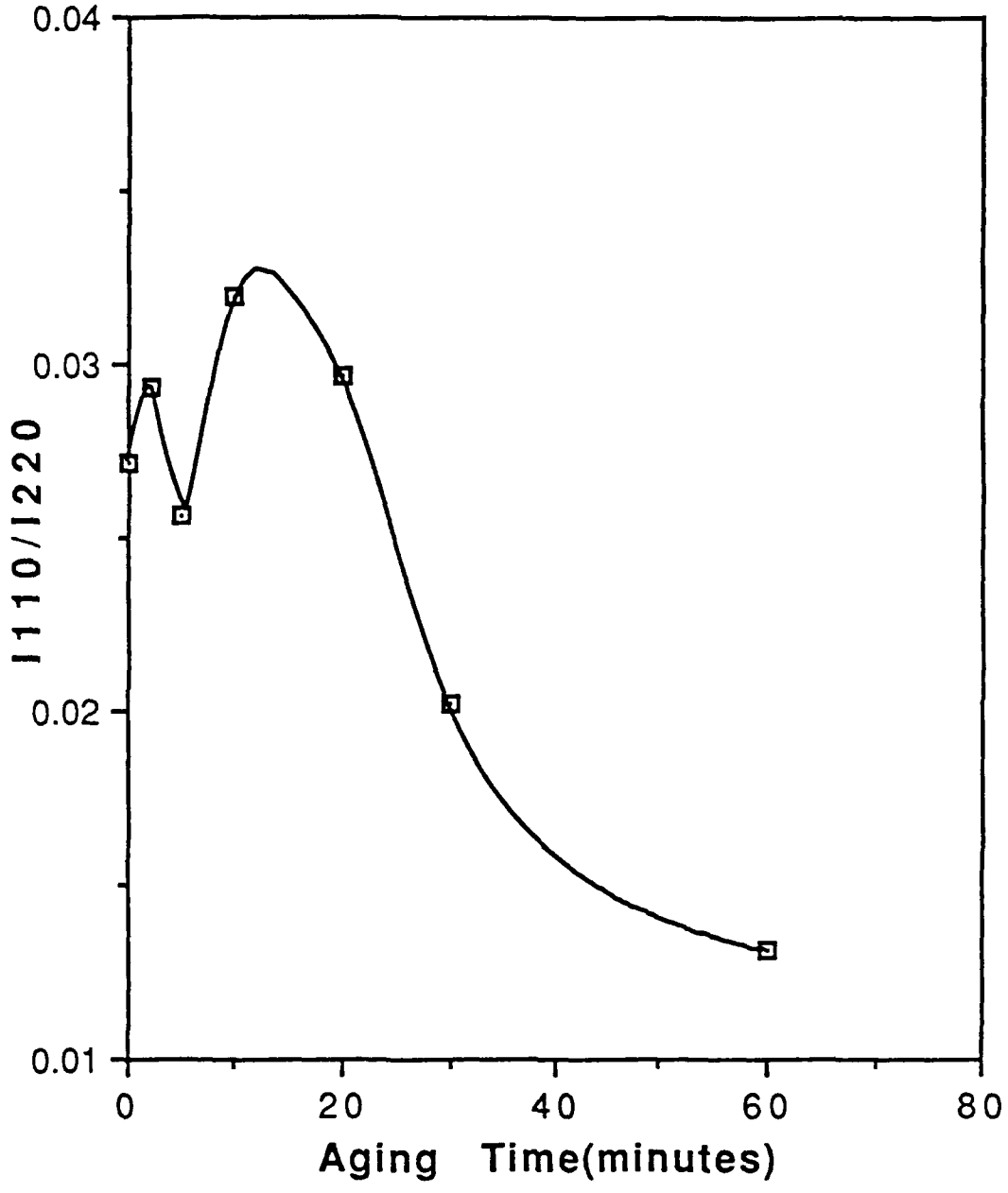

Figure 14. I_{110} / I_{220} versus Aging Time (Al-Li binary).

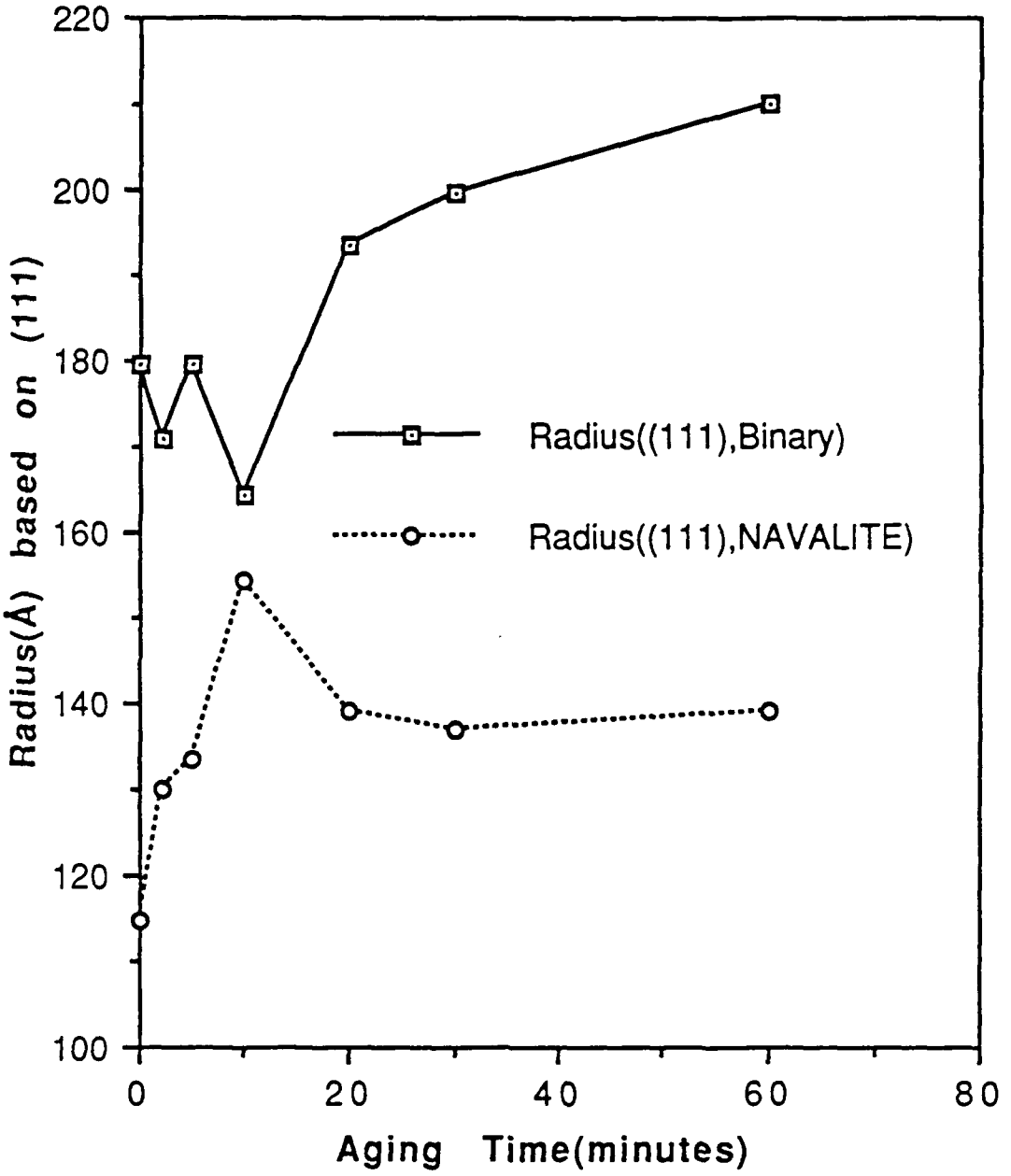

Figure 15. Intensity of 111 peak versus Aging Time.

D. ERROR ANALYSIS

The accuracy of an XRD analysis is dependent on the method used for measuring intensity and breadth of the diffraction profile. The major error comes from the determination of background. As the error in the breadth of the pure profile is directly proportional to particle size error, the following error expression was used to determine the particle size error [Ref. 40:p. 361-364]:

$$\frac{d\beta}{\beta} = \frac{\sqrt{N_e}}{N_e} + \frac{dh_e}{h_e} + \frac{\sqrt{N_s}}{N_s} + \frac{dh_s}{h_s}$$

β = pure profile breadth.

N_e= No. of counts under experimental peak.

h_e= Height of experiment peak.

N_s= No. of counts under quartz standard peak.

h_s= Height of quartz standard peak.

dh_s= .lin (accuracy of measurement).

Appendices A and B consist of complete error analysis of both alloys for all aging times. By comparing particle size errors with Whitman's results (plate sample) [Ref. 1], it can be seen that particle size errors in the current powder samples are somewhat smaller.

TABLE 3. PARTICLE SIZE ERROR (BASED ON I_{100})

Heat Treatment Time (minutes)	Particle Size Error (%,Al-Li binary)	Particle Size Error (%,Navalite)
As-Quenched	6.51	6.32
2	4.88	--
5	4.26	--
10	4.23	--
20	4.29	--
30	4.26	--
60	4.23	--

V. CONCLUSIONS

Powders are superior to plate samples for X-ray diffraction of Al-Li alloys, as preferred orientation and lithium loss effects are avoided. The powder XRD experiments give excellent results for determination of the volume fraction and particle size of δ' in the as-quenched condition. For the as-quenched binary alloy, the microstructure can be modeled as a two-phase region including a 50.5% ordered phase with a 43Å particle size and a disordered phase. The microstructure of as-quenched Navalite appears to be nearly fully ordered with about 90% δ' particles of size 38Å in a matrix of 10% disordered phase.

These two alloys were found to have degrees of order higher than those predicted by theory. This implies that the congruent order-disorder transformation followed by the spinodal decomposition transformation path suggested by Khachaturyan et al. is likely. Another factor contributing to the high volume fraction of the as-quenched alloy is the addition of Mg and Cu, promoting δ' precipitation upon quenching.

The aging characteristics of δ' in binary Al-Li followed Ostwald ripening kinetics. However, the ordered phase of as-quenched Navalite rapidly disappeared after aging as δ' was replaced by other phases such as $T_1(Al_2CuLi)$ and $S(Al_2CuMg)$.

The presence of δ was observed in the as-quenched binary Al-Li and subsequently coarsened during the aging heat treatment. No δ (Al-Li) was found in as-quenched Navalite or after any of the artificial aging heat treatments. The Navalite results showed the larger line breadth of fundamental peak profiles, indicating that Navalite has a finer microstructure compared to binary Al-Li. The above results conclusively show that alloying elements promote δ' nucleation and refine the microstructure.

VI. RECOMMENDATIONS

The following recommendations are given for further study in Al-Li based alloys:

* The improvement of diffraction profile measurements, if possible, by computer-assisted intensity calculations. This would be far more accurate than weighing the plotter paper.
* Further research into increased time aging characteristics and into the ordered phase of as-quenched Navalite in order to observe the effects of alloying element additions.
* The δ phase could not be avoided in the as-quenched binary alloy, whereas it was not evident in Navalite. This suggests that alloying additions give the additional benefit of the avoidance of δ.
* XRD analysis using powder samples gives excellent results. However, this method should be performed on several samples for greater statistical accuracy.

APPENDIX A. EXPERIMENTAL RESULTS (AL-LI BINARY)

TABLE 4. AS-QUENCHED DATA

Peak(hkl and phase)	Intensity (counts)	Integral Breadth (rads)	Particle Size(Å)	Particle Size Error in percent
100(δ')	4700	0.039060	43.3	6.51
111(δ)	501	0.0044795	464	9.68
110(δ')	3923	0.028503	61	7.25
111	358182	0.005631	359	4.07
220(δ)	1389	0.010099	182	7.51
200	194721	0.006426	316	3.60
220	144401	0.008115	265	3.19
311	174673	0.009676	246	2.83
222	50954	0.010004	246	3.13

TABLE 5. 2 MINUTES AGE DATA

Peak(hkl and phase)	Intensity (counts)	Integral Breadth (rads)	Particle Size(Å)	Particle Size Error in percent
100(δ')	4297	0.037367	59.6	4.88
111(δ)	799	0.006640	277	8.41
110(δ')	4296	0.027767	62.4	6.75
111	335502	0.005847	342	2.27
220(δ)	1549	0.009483	194	6.75
200	184731	0.006612	288	3.8
220	145906	0.008934	236	3.33
311	183322	0.010353	226	2.86
222	52376	0.009989	246	2.91

TABLE 6. 5 MINUTES AGE DATA

Peak(hkl and phase)	Intensity (counts)	Integral Breadth (rads)	Particle Size(Å)	Particle Size Error in percent
100(δ')	5605	0.028352	65.3	4.63
111(δ)	846	0.006152	304	7.75
110(δ')	4670	0.029366	59	6.59
111	334092	0.005633	359	2.23
220(δ)	1641	0.009088	204	6.36
200	181443	0.006301	324	3.73
220	134812	0.008002	269	3.29
311	163486	0.009323	257	2.88
222	49427	0.009664	257	2.96

TABLE 7. 10 MINUTES AGE DATA

Peak(hkl and phase)	Intensity (counts)	Integral Breadth (rads)	Particle Size(Å)	Particle Size Error in percent
100(δ')	5274	0.023598	71.9	4.35
111(δ)	987	0.0063797	291	7.05
110(δ')	4465	0.025341	68.4	6.29
111	328569	0.006019	329	2.33
220(δ)	1760	0.008904	209	6.01
200	175332	0.006580	306.6	3.93
220	139607	0.008545	497.7	3.34
311	166916	0.009707	244	2.91
222	50414	0.009775	253	2.94

TABLE 8. 20 MINUTES AGE DATA

Peak(hkl and phase)	Intensity (counts)	Integral Breadth (rads)	Particle Size(Å)	Particle Size Error in percent
100(δ')	4712	0.019862	85.7	4.29
111(δ)	794	0.006601	279	8.42
110(δ')	3979	0.024363	71	6.62
111	319404	0.005327	387	2.22
220(δ)	1908	0.009251	200	5.81
200	169926	0.005901	354	3.74
220	134201	0.007885	274	3.27
311	164660	0.009483	252	2.90
222	47899	0.009525	262	2.99

TABLE 9. 30 MINUTES AGE DATA

Peak(hkl and phase)	Intensity (counts)	Integral Breadth (rads)	Particle Size(Å)	Particle Size Error in percent
100(δ')	4256.4	0.017074	100	4.26
111(δ)	966	0.006145	304	8.09
110(δ')	3375	0.018696	93	6.44
111	304713	0.005213	399	2.25
220(δ)	1734	0.008407	222	5.92
200	166986	0.006024	344	3.83
220	125928	0.008371	255	3.50
311	162780	0.009375	255	2.90
222	48181	0.009664	257	3.00

TABLE 10. 1 HOUR AGE DATA

Peak(hkl and phase)	Intensity (counts)	Integral Breadth (rads)	Particle Size(Å)	Particle Size Error in percent
100(δ')	4030	0.015630	109.6	4.23
111(δ)	1128	0.007720	233	7.05
110(δ')	2696	0.013635	130	6.39
111	284031	0.005025	420	2.30
220(δ)	1716	0.088708	209	6.11
200	153942	0.005872	356	3.99
220	120710	0.006884	325	3.24
311	157375	0.009063	267	2.91
222	47006	0.009594	259	3.03

APPENDIX B. EXPERIMENTAL RESULTS (NAVALITE)

TABLE 11. AS-QUENCHED DATA

Peak(hkl and phase)	Intensity (counts)	Integral Breadth (rads)	Particle Size(Å)	Particle Size Error in percent
100(δ')	5279	0.043864	38.58	6.32
111	250187	0.008141	229.4	2.22
200	156716	0.010185	184.4	3.14
220	120123	0.012704	159.8	3.14
311	137350	0.015145	146.5	2.85
222	44115	0.014663	157.2	3.92

TABLE 12. 2 MINUTES AGE DATA

Peak(hkl and phase)	Intensity (counts)	Integral Breadth (rads)	Particle Size(Å)	Particle Size Error in percent
100(δ')	--	--	--	--
111	338676	0.007296	260	2.55
200	178762	0.008523	225	2.65
220	136340	0.011170	184	2.80
311	153121	0.013195	170	2.50
222	47922	0.012816	183	3.45

TABLE 13. 5 MINUTES AGE DATA

Peak(hkl and phase)	Intensity (counts)	Integral Breadth (rads)	Particle Size(Å)	Particle Size Error in percent
100(δ')	--	--	--	--
111	257709	0.007138	267	3.00
200	138244	0.008376	229	3.04
220	110863	0.011215	183	3.09
311	131615	0.012976	174	2.69
222	41624	0.013451	173	3.87

TABLE 14. 10 MINUTES AGE DATA

Peak(hkl and phase)	Intensity (counts)	Integral Breadth (rads)	Particle Size(Å)	Particle Size Error in percent
100(δ')	--	--	--	--
111	258531	0.006332	309	2.78
200	146610	0.008485	226	2.95
220	111591	0.011096	185	3.06
311	144941	0.013382	168	2.59
222	41483	0.012784	183	3.78

TABLE 15. 20 MINUTES AGE DATA

Peak(hkl and phase)	Intensity (counts)	Integral Breadth (rads)	Particle Size(Å)	Particle Size Error in percent
100(δ')	--	--	--	--
111	326220	0.006900	278	2.53
200	181818	0.008393	229	2.60
220	131240	0.010828	190	2.81
311	161135	0.013390	168	2.45
222	46524	0.011515	207	3.55

TABLE 16. 30 MINUTES AGE DATA

Peak(hkl and phase)	Intensity (counts)	Integral Breadth (rads)	Particle Size(Å)	Particle Size Error in percent
100(δ')	--	--	--	--
111	310590	0.006982	274	2.62
200	165366	0.008083	239	2.69
220	129313	0.011061	186	2.85
311	156857	0.013517	166	2.50
222	47993	0.0013958	166	3.62

TABLE 17. 1 HOUR AGE DATA

Peak(hkl and phase)	Intensity (counts)	Integral Breadth (rads)	Particle Size(Å)	Particle Size Error in percent
100(δ')	--	--	--	--
111	305301	0.006896	278	2.63
200	167058	0.008031	241	2.67
220	129806	0.010943	188	2.83
311	157868	0.013454	167	2.49
222	67053	0.018141	125	3.41

APPENDIX C. INSTRUMENTAL BROADENING (BASED ON QUARTZ STANDARD)

TABLE 18. QUARTZ STANDARD DATA

Position (2θ)	Intensity (counts)	Integral Breadth (radians)	Total Fractional Error
20.98	20057	0.002745	0.02589
26.6	114642	0.00247	0.01777
31.1	3085	0.0033	0.05436
36.6	11958	0.0028	0.02547
39.6	12766	0.0028	0.02377
42.5	10118	0.0031	0.03113
45.7	7247	0.0030	0.04006
50.4	29210	0.0032	0.02109
60.0	25105	0.0037	0.01644
64.2	4846	0.0032	0.03698
75.7	9614	0.0041	0.02488
83.7	6944	0.0045	0.03422

LIST OF REFERENCES

1. Whitman, C. E., "An Investigation of Delta Prime Growth in an Aluminum-lithium Alloy using X-ray Diffraction Analysis", Masters Thesis, Naval Postgraduate School, Monterey, Ca., March 1990.

2. Fuller, S. J., "An Investigation of the As-quenched and Early Aging Characteristics of a Al-4.1 wt.%Li Binary Alloy by X-ray Diffraction", Masters Thesis, Naval Postgraduate School, Monterey, Ca., June 1990.

3. Balmuth, E. S. and Schmidt, R., "A Perspective on the Development of Aluminum-Lithium Alloys", *Aluminum-Lithium Alloys*, Sanders, T. H. and Starke, E. A., eds., The Metallurgical Society of AIME, 1981.

4. Prichett, T. R., "Advanced Technology Aluminum Materials for Aerospace Applications", *Aluminum Technology '86.*, Sheppard, T., ed., Institute of Metals, 1986.

5. Roy, G., "Status of Al-Li Development at Pechiney", *Al-Li Conference, March 25-26, 1987, Los Angeles, Ca.*, Ramesh, J., Suphal, P., and Quist, W. eds., ASM 1987.

6. Little, D., "Overview", *Al-Li Alloys III, University of Oxford, 8-11 July 1985*, Gregson, P. J., Harrison, S.J., and Peel, C. J., eds., Institute of Metals, London, 1986.

7. Forness, S. and Heckman, E. A. W., "The Use of 8090 in the McDonell-Douglas F15 SMTD Aircraft", *Al-Li Conference, March 25-26, 1987, Los Angeles, Ca.*, Ramesh, J., Suphal, P., and Quist, W. eds., ASM 1987.

8. Peel, C. J., and others, "The Development and Application of Improved Al-Li Alloys", *Aluminum-Lithium Alloys II*, Sanders, T. H. and Starke, E. A., eds., The Metallurgical Society of AIME, 1984.

9. Wadsworth, J., "Superplasticity Behavior of Al-Li Alloys", *Aluminum-Lithium Alloys II*, Sanders, T. H. and Starke, E. A., eds., The Metallurgical Society of AIME, 1984.

10. Pickens, J. R., Heubaum, F. H., and Kramer, L. S., "Ultra-high-strength, Forgeable Al-Cu-Li-Ag-Mg Alloy", *Scripta Met.* Vol. 24, pp. 457-462, 1990.

11. Averill, W. A., Olson, D. L., Matlock, D. K., and Edwards, G. R., "Lithium Reactivity and Containment", *Aluminum-Lithium Alloys*, Sanders, T. H. and Starke, E. A., eds., The Metallurgical Society of AIME, 1981.

12. Sigli, C. and Sanchez, J. M., "Calculation of Phase Equilibria in Al-Li Alloys", *Acta. Metall.*, Vol. 34, No. 6, pp. 1021-1028, 1986.

13. Baumann, S. F. and Williams, D. B., "Effects of Capillarity and Coherency on δ' (Al_3Li) precipitation in Dilute Al-Li Alloys on Low Undercoolings", *Acta. Metall.*, Vol. 33, No. 6, pp. 1069-1078, 1985.

14. Furukawa, M., Miura, Y., and Nemoto, M., "Strengthening Mechanisms in Al-Li Alloys Containing Coherent Ordered Particles", *Trans. JIM.*, Vol. 26, No. 4, pp. 230-235, 1985.

15. Furukawa, M., Miura, Y., and Nemoto, M., "Arrangement of Deformation Induced Dislocations in Aged Al-Li Alloys", *Trans. JIM.*, Vol. 26, No. 4, pp. 225-229, 1985.

16. Sanders, T. H. and others, "The $\delta'(Al_3Li)$ Particle Size Distributions in a Variety of Al-Li Alloys", *Aluminum-Lithium Alloys III*, Sanders, T. H. and Starke, E. A., eds., The Metallurgical Society of AIME, 1986.

17. Gu, B. P., Liedl, G. L., Kulwicki, J. H., and Sanders, T. H., "Coarsening of Delta Prime Precipitates in an Al-2.8Li-0.3Mn Alloy", *Mat. Sci. Eng.*, Vol. 70, pp. 217-228, 1985.

18. Jha, S. C., Sanders, T. H., and Dayananda, M. A., "Grain Boundary Precipitate Free Zones in Al-Li Alloys", *Acta. Metall.*, Vol. 35, No. 2, pp. 473-482, 1987.

19. Williams, D. B., "Microstructural Characteristics of Al-Li Alloys", *Aluminum-Lithium Alloys*, Sanders, T. H. and Starke, E. A., eds., The Metallurgical Society of AIME, 1981.

20. Quist, W. E., Narayanan, G. H., and Wingert, A. L., "Al-Li Alloys for Aircraft Structure--An Overview", *Aluminum-Lithium Alloys II*, Sanders, T. H. and Starke, E. A., eds., The Metallurgical Society of AIME, 1984.

21. Sanders, T. H. and Starke, E. A., "Overview of the Physical Metallurgy in the Al-Li-X System", *Aluminum-Lithium Alloys II*, Sanders, T. H. and Starke, E. A., eds., The Metallurgical Society of AIME, 1984.

22. Dinsdale, K., Harris, S. J., and Noble, B., "Relationship Between Microstructure and Mechanical Properties of Aluminum-Lithium-Magnesium Alloys", *Aluminum-Lithium Alloys*, Sanders, T. H. and Starke, E. A., eds., The Metallurgical Society of AIME, 1981.

23. Lavernia, E. J., Srivatsan, T. S., and Mohamed, F. A., "Review on Strength, Deformation, Fracture Behavior and Ductility of Aluminum-Lithium Alloys", *Met. Sci.* Vol. 25, No. 2B, pp. 1137-1158, Feb. 1990.

24. Gregson, P. J. and Flower, H. M., "δ' Precipitation in Al-Li-Mg-Cu-Zr Alloys", *J. Mat. Sci. Letters*, 3, pp. 829-834, 1984.

25. Khachaturyan, A. G., Lindsey, T. F., and Morris, J. W., "Theoretical Investigation of the Precipitation of δ' in Al-Li", *Met. Trans. A*, Vol. 19A, Feb. 1988.

26. Radmilovic, V., Fox, A. G., and Thomas, G., "Spinodal Decomposition of Al-Rich Al-Li Alloys", *Acta. Metall.*, Vol. 37, No. 9, pp. 2385-2394, 1989

27. Williams, D. B. and Edington, J. W.,"The Precipitation of $\delta'(Al_3Li)$ in Dilute Aluminum-Lithium Alloys", *Metal Science*, Vol. 9, pp. 529-532, 1975.

28. Gayle, F. W. and Vandersande, J. B., "*Bull. Alloy Phase Diagram*", Vol. 5, p. 19, 1984.

29. Flower, H. M. and Gregson, P. J., "Solid State Phase Transformations in Aluminum Alloys Containing Lithium", *Mat. Sci. Tech.*, 3, pp. 81-90, 1987.

30. Sato, T., Tanaka, N., and Takahashi, T., "High Resolution Lattice Images of Ordered Structures in Al-Li Alloys", *Trans. JIM*, Vol. 29, No. 1, pp. 17-25, 1988.

31. Spooner, S., Williams, D., and Sung, C., "Combined Small Angle X-Ray Scattering and Transmission Electron Microscopy Studies of Al-Li Alloys", *Al-Li Alloys III, University of Oxford, 8-11 July 1985*, Gregson, P. J., Harrison, S. J., and Peel, C. J., eds., Institute of Metals, London, 1986.

32. Starke Jr., E. A., "Strength of Metals and Alloys", *Proceeding of the Sixth International Conference*, Pergamon Press, p. 1025, 1983.

33. Fox, A. G. and Fisher, R. M., "Structure Factors and Debye Temperature of Al-Li Solid-Solution Alloys", *Acta. Cryst.*, A43, pp. 260-265, 1987.

34. Fox, A. G. and Fisher, R. M., "The Origin of the High Elastic Modulus in Al-Li Alloys", *J. Mat. Sci. Letters*, 7, pp. 301-303, 1988.

35. Noble, B., Harris, S. J., and Dinsdale, K., "Yield Characteristics of Aluminum-Lithium Alloys", *Met. Sci.* Vol. 16, No. 9, Sept., 1982

36. Sanders, T. H. and Starke, E. A., "The Effects of Slip Distribution on the Montonic and Cyclic Ductility of Al-Li Binary Alloys", *Acta. Metall.*, Vol. 30, pp. 927-939, 1982.

37. Sung, C. M., Chan, H. M., and Williams, D. B., "Quantitative Microanalysis of Li in binary Al-Li Alloys", *Al-Li Alloys III, University of Oxford, 8-11 July 1985*, Gregson, P. J., Harrison, S. J., and Peel, C. J., eds., Institute of Metals, London, 1986.

38. Pickering, H. W., "(1) Atomistic Study of Metastable Phases in an Al-3 wt.%Li-0.12 wt.%Zr Alloy, (2) A Preliminary Study of Al-Li Alloys using Atom Probe Field Ion Microscopy and Transmission Electron Microscopy", *Office of Naval Research Technical Report No. N00014-84-k-0201, 2 March 1987.*

39. Chan, H. M. and Williams, D. B., "Quantitative Analysis of Lithium in Al-Li Alloys by Ionization Energy Loss Spectroscopy", *Phil. Mag.*, Vol. 52, No. 5, pp. 1019-1032, 1985.

40. Klug, H. P. and Alexander, L. E., *X-Ray Diffraction Procedures*, Chap. 9, John Wiley and Sons, 1974.

INITIAL DISTRIBUTION LIST

		No. Copies
1.	Library, Code 52 Naval Postgraduate School Monterey, CA. 93943-5002	2
2.	Naval Engineering Curricular Office, Code 34 Naval Postgraduate School Monterey, CA. 93943-4004	1
3.	Prof. A. J. Healy, Code ME/HY Chairman Department of Mechanical Engineering Naval Postgraduate School Monterey, CA. 93943-5100	1
4.	Prof. A. G. Fox, Code ME/FX Department of Mechanical Engineering Naval Postgraduate School Monterey, CA. 93943-5100	3
5.	Prof. Terry R. McNelley, Code ME/MC Department of Mechanical Engineering Naval Postgraduate School Monterey, CA. 93943-5100	1
6.	Department of Mechanical Engineering Chung Cheng Institute of Technology Tao-Yuan, Tai-Hsi Taiwan, R.O.C.	1
7.	Capt. Te-Kang Wang, Taiwan (R.O.C.) Army P.O. Box 90047-23 Tashih, Tao-Yuan, Taiwan Republic of China	3
8.	Defense Technical Information Center Cameron Station Alexandria, VA 22304-6145	2